

A Study of I–III–VI₂ Semiconductor Quantum Dots

A thesis submitted to

Indian Institute of Science Education and Research, Pune

for partial fulfillment of
BS-MS Dual Degree Program



By

Ranjana Yadav (20141025)

Under the supervision of

Dr. Anshu Pandey

Associate Professor,

Department of Solid State and Structural Chemistry Unit,

Indian Institute of Science, Bangalore, India

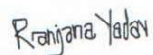
Dedicated
To
My Beloved Parents

Certificate

This is to certify that this thesis entitled 'A Study of I-III-VI₂ Semiconductor Quantum Dots' towards the partial fulfilment of the BSMS dual degree program at the Indian Institute of Science Education and Research, Pune represents the work carried out by Ranjana Yadav at Indian Institute of Science (IISc) under the supervision of Dr. Anshu Pandey, Associate Professor, Solid State and Structural Chemistry Unit (SSCU) during the academic year 2018-1019.

Date: 10/03/2019

Place: Pune



Ranjana Yadav

BS-MS

Chemistry



Dr. Anshu Pandey

Associate Professor

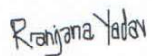
SSCU, IISc

Declaration

I hereby declare that the matter embodied in the report entitled "A Study of I-III-VI₂ Semiconductor Quantum Dots" are the results of the work carried out by me at the Department of Solid State and Structural Chemistry Unit, Indian Institute of Science, under the supervision of Dr. Anshu Pandey and the same has not been submitted elsewhere for any other degree.

Date: 10/03/2019

Place: Pune



Ranjana Yadav

BS-MS

Chemistry



Dr. Anshu Pandey

Associate Professor

SSCU, IISc

Acknowledgement

First and foremost, I would like to express my sincere gratitude towards my master's thesis guide, Dr. Anshu Pandey for giving me an opportunity to carry out the project under his supervision and his support throughout the year. He steered me in the right direction whenever I needed it. Working under his guidance has been an absolute honor.

I'd also like to thank my thesis adviser committee member, Dr. Pramod Pillai for his support throughout my project and my stay at IISER.

I would like to thank Dr. Biswajit Bhattacharya for guiding me throughout the project and helping me in spectroscopic measurements. I would also like to thank my lab members Dr. Rekha, Arpita, Dr. Nihit, Subham, Biman, Pritha, Anumol, Pranab, Dev, Guru and Nitin for their valuable assistance and motivation throughout the course of IISc stay. It was truly a pleasure working alongside them.

Last but not the least, I would like to thank my mom, dad, my family, my dear friends Komal, Supriya, Suknya, Shardha, Suraj and Shubham for being a part of my IISER life and giving me encouragement in my hard time. I am really thankful to my closest friend Amit for his unconditional love and support throughout my IISER journey. I owe my deepest gratitude to each of you.

Contents

List of Figures.....	8
Abbreviations.....	9
Abstract.....	10
Chapter 1 Introduction.....	11
1.1. Quantum dots.....	12
1.2. Core/ shell structure based quantum dots.....	13
1.3. I–III–VI ₂ ternary quantum dots.....	15
1.4. Motivation.....	15
Chapter 2 Synthesis and Characterization of Core Shell structure based CuAl _x Fe _{1-x} S ₂ alloyed Quantum Dots.....	17
2.1 Introduction.....	18
2.2 Experimental Section.....	18
2.2.1 Materials.....	18
2.2.2 Synthesis of CuAl _x Fe _{1-x} S ₂ and core/shell.....	18
2.3 Instrumental characterization.....	19
2.3.1 UV-Vis-NIR Absorbance.....	19
2.3.2 Photoluminescence Study.....	20
2.3.3 X-ray diffraction (XRD).....	20
2.3.4 Transmission electron microscopy (TEM) and High resolution TEM (HRTEM).....	21
2.3.5 Energy dispersive X-ray analysis (EDX) and STEM elemental mapping.....	21
2.3.6 Quantum yield and life time measurement.....	22
2.3.7 X-ray photoelectron spectroscopy (XPS)	22
2.3.8 Inductively Coupled Plasma Atomic Emission Spectroscopy (ICP- AES).....	22

2.4 Results and Discussion.....	23
2.4.1 Crystal Structural analysis.....	23
2.4.2 Composition Analysis.....	25
2.4.3 Optical characterization.....	26
2.5 Conclusion.....	30
Chapter 3 Synthesis and Characterization of CuAlS ₂ /Ga ₂ S ₃ Quantum Dots.....	31
3.1 Introduction.....	32
3.2 Experimental Section.....	32
3.2.1 Materials.....	32
3.2.2 Synthesis.....	33
3.1 Instrumental characterization.....	33
3.2 Results and Discussion.....	34
3.2.1 Structural characterization.....	34
3.2.2 Optical characterization.....	35
3.3 Conclusion.....	37
References.....	38

List of Figures

1. Tunable photoluminescence of quantum dots with size	13
2. Different types of core shell structure based quantum dots.....	14
3. X-ray pattern, unit cell of I-III-VI ₂ chalcopyrite crystal structure and a schematic of its energy band diagram.....	23
4. TEM images, HRTEM images, Histogram of the particle size distribution of alloyed QDs.....	25
5. EDAX spectrum and STEM Elemental mapping of CuAl _{0.4} Fe _{0.6} S ₂ QDs.....	26
6. Absorbance spectrum of core QDs with different compositions.....	27
7. Absorbance spectrum of CuAl _x Fe _{1-x} S ₂ /ZnS with different composition of iron and aluminum. Photoluminescence spectrum of core shell QDs.....	28
8. Example of tauc plot which is used in calculation of direct band gap of alloyed QDs and decay profile of core shell QDs.....	29
9. X-ray diffraction of CuAlS ₂ , CuAlS ₂ /Ga ₂ S ₃ , standard pattern of CuAlS ₂ and Ga ₂ S ₃	34
10. High resolution TEM images, TEM images, FFT of HRTEM images and EDAX of CuAlS ₂ /Ga ₂ S ₃	35
11. Absorbance spectrum and photoluminescence spectrum of CuAlS ₂ / Ga ₂ S ₃	36

List of Abbreviation

- | | | |
|-----|----------|---|
| 1. | NPs | Nanoparticles |
| 2. | QDs | Quantum Dots |
| 3. | CSQDs | Core shell quantum dots |
| 4. | PL | Photoluminescence |
| 5. | XRD | X-ray diffraction |
| 6. | TEM | Transmission Electron Microscopy |
| 7. | STEM | Scanning Transmission Microscopy |
| 8. | HRTEM | High Resolution Transmission Microscopy |
| 9. | XPS | X-ray Photoelectron Microscopy |
| 10. | ICP(AES) | Inductively Coupled Plasma Atomic Emission Spectroscopy |
| 11. | QY | Quantum Yield |
| 12. | FFT | Fast Fourier Transformation |

Abstract

I-III-VI₂ semiconductors are being widely investigated due to their various possible applications in photovoltaics, LEDs, bio-imaging etc. These ternary semiconductors exhibit unique optical and photo physical properties depending on their composition, size and their large non-stoichiometric structural tolerance. However, mostly studied ternary quantum dots are based on In, Ga, Se, Te and Cd, confronts major issues in practical applications because of their toxic composition or use of rare earth elements. In recent development, these rare or toxic elements are being substituted with a non-toxic and earth profuse elements as iron, aluminum etc. to overcome the above mentioned problem. Here we have studied synthesis, structural and optical characterizations of ternary semiconductor QDs which contain earth abundant and nontoxic compositions. Alloying iron into CuAlS₂ quantum dots reveals a shift in band gap of the material from UV to near IR region. It was observed that a wide band gap II-VI semiconductor shell coating over the alloyed core CuAl_xFe_{1-x}S₂ enhanced the photoluminescence which range from 580nm-1050nm with the change in ratio of iron and aluminum. PL decay for alloyed samples revealed a defect mediated long lifetime similar as expected for this class of material. The observed PLQY is more than 3% in some cases. A large stoke shift is observed throughout all the compositions of CuAl_xFe_{1-x}S₂/ZnS. Due to its nontoxic compositions and emission in NIR region, the studied material could be a potential candidate for bio-imaging and bio-detection.

Chapter-1

Introduction

Introduction

The development of high efficiency and low cost photovoltaics is driven by the continuous demand of energy¹. There are global need for environment-friendly, cheap, clean and renewable energy sources as alternatives for traditional energy sources²⁻⁵. The main problem with fossil fuels is that they are non-renewable and are in a limited amount. There is high use of fossil fuels in recent decades which cause serious damage to the environment. Therefore, obtainable resources are urgently needed. In this regard, solar energy is a more feasible and effective option. To use the solar energy, we need to design materials with suitable properties and performance¹⁻⁴. One of the major concerns has been sustainability and compositions of these materials^{4,5,14}. Earth abundant and benign composition of material with large scale up synthetic approach is our ultimate goal for this purpose.

Nanoparticle semiconductor materials have very interesting properties which are significantly different from their bulk materials². In the regard of structure and size, nanoparticles act as a bridge between bulk and atoms, however, their properties are distinct from either². The reduction in size leads to quantum confinement². This effect causes change in the opto-electronic and photo-physical properties of the material depending on its size².

1.1 Quantum Dots

Quantum dots (QDs), also known as artificial atoms are semiconductor nanocrystals in which electrons are specially confined in all three directions within a potential barrier. This confinement occurs when size of a particle become less than its Bohr's diameter. This quantum confinement effect can be realized by a particle in a box example. These semiconductor quantum dots exhibit discrete energy levels that can be controlled. The energy band gap (E_g) of QDs can be tuned with size because of the quantum confinement phenomenon. A smaller size quantum dot has stronger confinement effect making its energy gap broader. Similarly, larger size quantum dots show narrow band gap.

Unlike many organic dyes, quantum dots have a continuous and broad absorption spectra with a narrower and more symmetric emission spectra. Therefore, quantum dots are more sensitive in detection than for organic dyes. Figure 1 exemplify size dependent Photoluminescence spectrum of core shell CdSe QDs. As shown in the figure 1, luminescence is sifted towards lower energy as size of the quantum dots are increased.

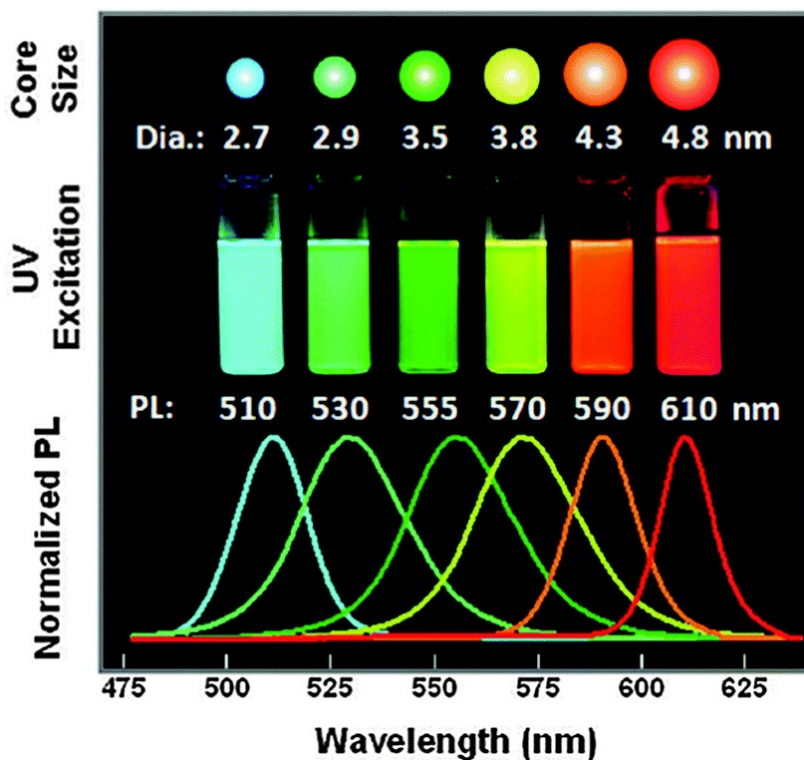


Figure 1) Tunable photoluminescence of CdSe/ZnS QDs¹⁰.

1.2 Core/Shell structure based quantum dots

Generally, organic surfactants are used to envelop the quantum dots. The dangling bond of the organic surfactant creates surface traps leading non-radiative recombination for excitons and hence a significant reduction in photoluminescence quantum yield (PLQY). To overcome this, a useful strategy could be encapsulation of core quantum dots with inorganic material. These types of quantum dots are known as core shell quantum dots (CSQDs).

There are different types of CSQDs exist depending upon their valance band and conduction band position such as type 1, inverse type1, type 2 and inverse type 2. In type 1, core material has a lower band gap than shell material. Figure 2 provides a schematic representation of different type of CSQDs. Depending on the requirement, absorbance of the CSQDs can be tuned by changing size of the core or the shell or both. It is also observed that the shell growth increases overall photo stability of quantum dots in some cases.

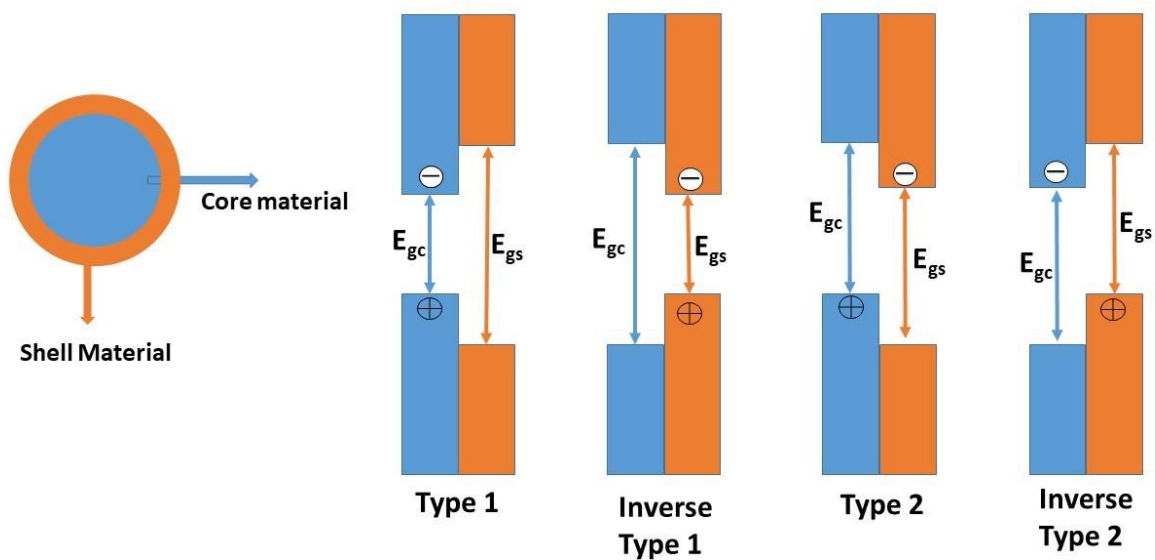


Figure 2) Different types of core/shell structure based QDs.

Mainly core/shell are composed of type II–VI, I–III–VI₂ and III–V semiconductor materials. For example CdS/ZnS, CuGaS₂/ZnS, CdSe/CdS, CuInS₂/CdS etc. There are many literatures available which provide an insight of various applications of CSQDs, such as in photovoltaics, bio imaging and LEDs³⁰⁻³⁴.

1.3 I–III–VI₂ ternary quantum dots

I–III–VI₂ QDs denote specific elemental compositions belonging to group-I such as copper (Cu), gold (Au), silver (Ag); III (any trivalent cation as indium (In), Gallium (Ga), Aluminium (Al) and VI consists sulphur (S), tellurium (Te), selenium (Se). This class of materials show wide tunability of optical band gaps starting from the ultraviolet to near infrared regions of the electromagnetic spectrum, depending on their elementary composition and crystal structure. This class of QDs offers a potentially less toxic alternative for replacing traditional toxic metal based materials.

Since past decades, there have been many reports on I–III–VI₂ QDs. They are gaining huge attention because of their applications in photovoltaics¹⁸, LEDs²⁶ and bio imaging^{10,13,17}. Most studied ternary materials are indium (In) based such as CuInS₂ and CuInGaSe₂ as thin film photovoltaics^{10,25,34}.

1.4 Motivation

Widely studied materials of I–III–VI₂ QDs are mainly composed of Indium, Selenium, Gallium and Tellurium which are rare and very expensive¹⁴⁻¹⁶. This seriously limits their practical applications. In this regards, ternary QDs which are based on light metals such as iron (Fe) and aluminum (Al) are potential candidates because of not only their environment friendly composition but also their earth abundance. CuFeS₂ is the only known non-toxic material composed of earth abundant elements with a narrow band gap (around 0.5 eV), which shows photoluminescence in IR^{6,19}. Another ternary class of material, CuAlS₂ is a wide band gap material with a bulk band gap of 3.45 eV shows a wide range of application such as in optical transparency³² and photo catalysis^{21,29}, depending on their core shell type structure. Therefore, in this thesis, I have tried to explore core shell structure based I–III–VI₂ quantum dots which contain nontoxic and earth abundant elements. Further, I have examined their optical and photo-physical properties.

In chapter 1, I have explored Fe and Al based alloy semiconductor material which could be a potential candidate in bio imaging. To obtain tunable light emission from UV to IR, I

have alloyed Fe into CuAlS₂ and have coated the core material with zinc sulfide to improve PL quantum yield.

In chapter 2, I have prepared CuAlS₂/Ga₂S₃ through colloidal route and studied its structural and optical properties. In a few previous studies, Ga₂S₃ has been used as a shell materials. It forms amorphous shell which improve overall stability of core material and suppress the surface defect.

Chapter-2

Synthesis and Characterization of Core Shell structure based $\text{CuAl}_x\text{Fe}_{1-x}\text{S}_2$ alloyed Quantum Dots

2.1 Introduction

I–III–VI₂ QDs are gaining huge attention as a replacement of traditional toxic element based quantum dots^{7,15}. This class of materials shows a wide range of tunability in optical band gaps¹². Ternary QDs like CuFeS₂ and CuAlS₂ are potential candidate because of their environment friendly composition. CuFeS₂ (bulk band gap around 0.5 eV) and CuAlS₂ (bulk band gap of 3.45 eV) are reported recently and both materials reveal unique and interesting properties. In recent studies, it was found that depending on their size and shell type, both ternary materials show their potential in various applications.

In this report, we have described the synthesis of CuAl_xFe_{1-x}S₂ and CuAl_xFe_{1-x}S₂/ZnS. To obtain tunable light emission from UV to IR, we have alloyed Fe into CuAlS₂ and have coated the core material with zinc sulfide to improve PL quantum yield as core material doesn't show any significant luminescence. Here we present a better understanding about structural and optical properties of ternary alloyed CuAl_xFe_{1-x}S₂ CSQDs which can be useful in different applications in future.

2.2 Experimental Section

2.2.1 Materials

Copper chloride (CuCl, 98%), Iron (III) acetylacetonate {Fe(acac)₃, 99%}, Aluminum acetylacetonate {Al(acac)₃, 99%}, elemental Sulphur (S), Zinc acetate {Zn(CH₃COO)₂, 99%}, 1-Octadecene (ODE, technical grade 90%), Oleic acid (OA, 90%), Oleylamine (technical grade, 70%), Dodecanethiol (DDT, 98%) were bought from Sigma-Aldrich. All the chemicals were used as they are received.

2.2.2 Synthesis

The synthesis of the alloyed QDs was carried out using slenkline setup. It consisted three steps.

In first step, anion precursor (Sulphur in Oleylamine 0.1M) and Zinc oleate (0.1M) was prepared. In a 30mL three-necked flask, elemental Sulphur (3.2 mg, 0.1mM), 2 mL Oleylamine and 2 mL of 1-octadecene was taken. This reaction mixture was heated at 160 °C under argon for 20 minutes. In another 50 mL flask, 548.78 mg of zinc acetate in oleic acid (15 mL) and Octadecene (10 mL) was added, and kept at 250 °C for 20 minutes under inert atmosphere for the preparation of zinc oleate (0.1 M).

In second Step we prepared ternary alloyed QDs with different ration of Aluminum and Iron. For a typical synthesis of $\text{CuAl}_{0.5}\text{Fe}_{0.5}\text{S}_2$, Iron acetylacetonate (35.5 mg, 0.1 mM), copper chloride (9.9 mg, 0.1 mM) and aluminum acetylacetonate (32.4mg, 0.1mM) were added to a 50 mL three necked flask containing 2 mL ODE as solvent and 2 mL oleic acid as ligand. The mixture was kept at 100 °C for 30 min to remove water under vacuum. Further, the metal precursors were heated under argon atmosphere at 180 °C for 20 min to dissolve the metal precursors. First, it formed a deep red color solution and after some time the iron starts dissolving and the color changes from red to brown color solution. Addition of 2 ml DDT at 180 °C turned reaction mixture color from brown to light yellow, initiating nucleation which is followed by growth. We observed that there is color change from light yellow to deep red which is associated with the growth of the core material.

In the third step, shell coating was done. At deep red color, reaction temperature was increased to 220°C. Simultaneously, 2ml of as prepared zinc oleate and 1 ml of S in OLM was added dropwise (duration 20 min). The solution was annealed for 10 mins then quenched in water bath.

The prepared QDs were cleaned several times with excess of methanol and ethanol to remove excess ligand and unreacted precursors. Further cleaned QDs were centrifuged at 1000 RPM to remove large particles. These cleaned QDs were uniformly dissolved in tetrachloroethylene (spectroscopic grade) for spectroscopic measurements.

2.3 Instrumental characterization

2.3.1 UV-Vis Absorption

The fundamental principles of UV-Vis spectroscopy for optical characterization of prepared QDs and instrumental set up has been described here. The UV-Visible spectroscopy is the most useful technique to find out the properties of QD like band gap, size distribution precisely. The optical absorption measurement of prepared samples has been performed in the spectral range of 190 to 2500 nm. Electromagnetic radiation generated from the source enters to the monochromator and then beam splits into two equal halves, one half passes through the reference and other half through the sample. The beam intensity passes through the references taken as 100% transmission or 0% absorption. The detector is synchronized with both the beams and it displays the ratio between the two beam intensities. The detector scans the incident photon energy across the desired range of the UV-Visible spectrum. QDs absorb the wave length of the light corresponding to its band gap. There are two absorption spectrometers are used to characterize the samples in this thesis, Ocean Optics and Perkin Elmer's Lambda 35 UV-Visible spectrometer.

2.3.2 Photoluminescence Study

Edinburg Instruments FLS920 Series Fluorescence Spectrometer with a 450W continuous Xe arc lamp as an excitation source was used for steady state photoluminescence (PL) measurements.

2.3.3 X- Ray Diffraction:

X- ray diffraction (XRD) provides important information about the structure, lattice parameter, composition and phase of a crystal system. The theory behind XRD is explained by Bragg's equation,

$$2d \sin \theta = n\lambda$$

Where :

d = Inter-planar distance

θ = Angle of diffraction

n = Order of diffraction

λ = Wavelength of incident X-ray

If x-ray diffraction satisfies the above condition then it leads to a constructive interference. The XRD pattern is recorded after scanning a range of 2θ angles.

Cleaned quantum dots were dissolved in hexane (spectroscopic grade) and drop casted on a glass substrate. It formed a homogenous film. Further, the film was washed with methanol and acetone two times. A 0.154 nm Cu K α x-ray source was used to collect the data.

2.3.4 Transmission Electron Microscopy and Scanning Transmission Electron Microscopy

Transmission electron microscopy (TEM) is a technique in which electron beams are transmitted through a very thin specimen. The interaction of the electrons with sample form an image which is magnified on imaging device and detected by a sensor. If these images are operated at the limit of resolution of the used instrument then it is known as a high resolution TEM (HRTEM).

The scanning transmission electron microscope (STEM) works similar as TEM but a very small beam of electrons is used to create an image.

Cleaned sample was dissolved in toluene and drop casted on copper TEM grids. HR-TEM images were obtained on a JEOL JEM-2100 transmission electron microscope (200 kV). An aberration corrected 250 kV TITAN TEM microscope was used for obtaining STEM.

2.3.5 Energy dispersive X-ray Analysis

Energy dispersive X-ray analysis (EDXA) is used for analysis of the elements or chemical composition of a specimen. In this technique, X-ray is used as source of excitation. Each element has a unique atomic structure which gives a unique set of peaks on its electromagnetic emission spectrum.

An aberration corrected 250 kV TITAN TEM microscope was used for obtaining STEM-EDX elemental mapping.

2.3.6 Quantum Yield and life time measurements:

A spectral coated integrating sphere on an Edinburgh Instruments, FLS 920 spectrofluorimeter was used to measure the absolute quantum yield in the VIS/NIR region. Beforehand, the sphere was calibrated with a standard UV/VIS/NIR light source to correct for any reflectivity artifacts. Samples were cleaned of all excess ligands and dissolved into an infrared compatible solvent (tetrachloro ethylene, TCE). An UV/VIS/IR transparent quartz cuvette containing TCE was introduced into the integrating sphere to determine lamp intensity and scattering characteristics of the sphere at excitation and emission wavelengths. An identical volume of the sample in TCE was subsequently put into the same cuvette and introduced into the sphere. The light absorbed and emitted is measured directly and the quantum yield is estimated as the light emitted to light absorbed. Time resolved PL data were collected in the self-same instrument. The sample emission was recorded using a laser diode excitation in right angle geometry.

2.3.7 X-ray photoelectron spectroscopy

X-ray Photoelectron spectroscopy (XPS) is a technique for surface characterization. A high energy x-ray source is used to excite electrons in specific bound state. Depending upon the transition energy, a specific binding energy can be calculated that can uniquely identify the element.

Substrates were cleaned with 1-propanol and acetone at 50 °C thoroughly five times to avoid any metal ion contamination. Then purified QDs were drop casted on to the

substrate. XPS spectra were measured by Kratos Axis Ultra Photo Electron Spectroscopy system with effective beam area of 20 micron.

2.3.8 Inductively Coupled Plasma Atomic Emission Spectroscopy (ICP-AES)

This technique is widely used in detection of chemical composition of a sample. It is an emission spectroscopic technique in which a high temperature argon plasma is used to pump electrons from the ground state to excited states. In process of returning back, they emit electromagnetic radiations at very specific wavelength. A calibration plot is used to determine unknown elemental concentrations.

ARCOS simultaneous ICP spectrometer, SPECTRO Analytical Instruments GmbH, Germany is used for the ICP- AES analysis of the alloyed quantum dots. All samples were prepared around 10 part per billion (PPB) of 10.

2.4 Results and Discussion

2.4.1 Structural characterization

Figure 3 exemplify the XRD pattern of $\text{CuAl}_x\text{Fe}_{1-x}\text{S}_2$ QDs along with the standard pattern of CuAlS_2 and CuFeS_2 . The intermediate peak positions of x-ray diffraction confirms that the core material is an alloy as per Vegard's law. XRD peaks are broadened due to the nano-scale size. It is observed that inter-planer distances are 0.33 and 0.19 which is corresponding to the (112) and (204) planes of a chalcopyrite crystal structure.

The core shell alloyed QDs show similar pattern as shell material ZnS (zinc blend structure). The absence of any secondary phases indicate the high structural purity of the QDs. Two zinc-blend unit cells which are stacked and compressed long the c axis form a chalcopyrite unit cell. In ternary system, two cations are in alternating positions along the c-axis replacing the cations of the corresponding III-V compound.

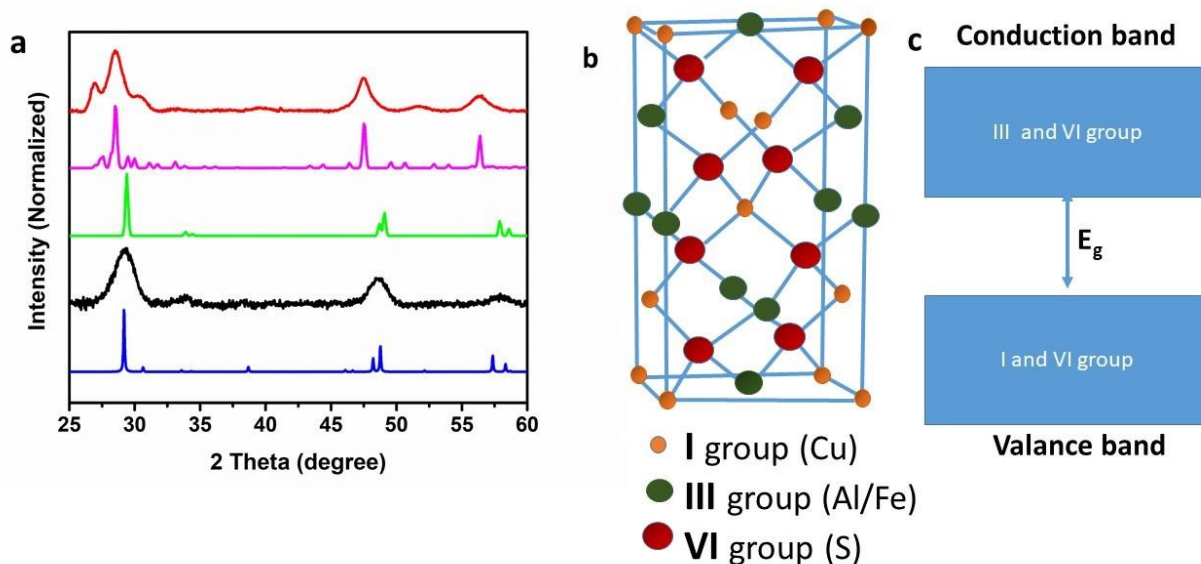


Figure 3a X-ray pattern of $\text{CuAl}_{0.4}\text{Fe}_{0.6}\text{S}_2$ QDs (black) and $\text{CuAl}_{0.4}\text{Fe}_{0.6}\text{S}_2/\text{ZnS}$ QDs (red), standard pattern of CuAlS_2 (Blue), standard pattern of CuFeS_2 (green) and standard pattern of ZnS zinc blend structure (pink). Unit cell of I–III–VI₂ chalcopyrite crystal structure (3b) and a schematic of its energy band diagram (3c).

Figure 4a and 4b show transmission electron micrographs (TEM) of alloyed quantum dots which suggest that the QDs are nearly monodisperse. High resolution TEM (HRTEM) shown in figure 4c and 4d. HRTEM exemplify a high quality single crystalline QDs. Figure 4e suggest that the average size of alloyed QDs is 5.5 ± 1.23 for all different compositions of iron and aluminum.

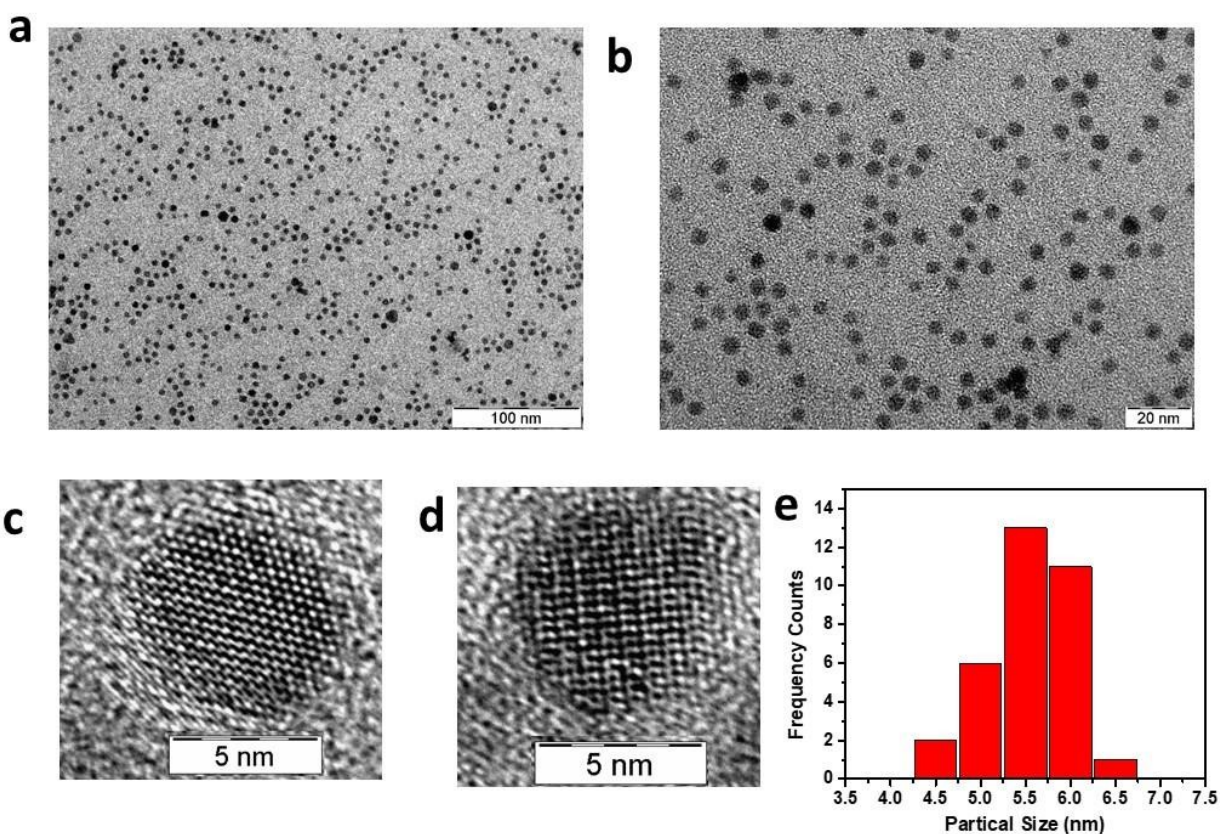


Figure 4) TEM images (a, b), HRTEM images (c, d) and Histogram of the particle size distribution (e) of $\text{CuAl}_{0.6}\text{Fe}_{0.4}\text{S}_2/\text{ZnS}$ QDs.

2.4.2 Compositional analysis

EDAX spectroscopy data of alloyed core quantum dots as well as coated with zinc sulfide one are shown in figure 5a and 5b respectively. STEM elemental mapping shown in figure 5c, reveals a homogenous distribution of Cu, Al, Fe and S in alloyed quantum dots. Composition was confirmed from ICP. A slight deviation was observed in composition in QDs that actual composition.

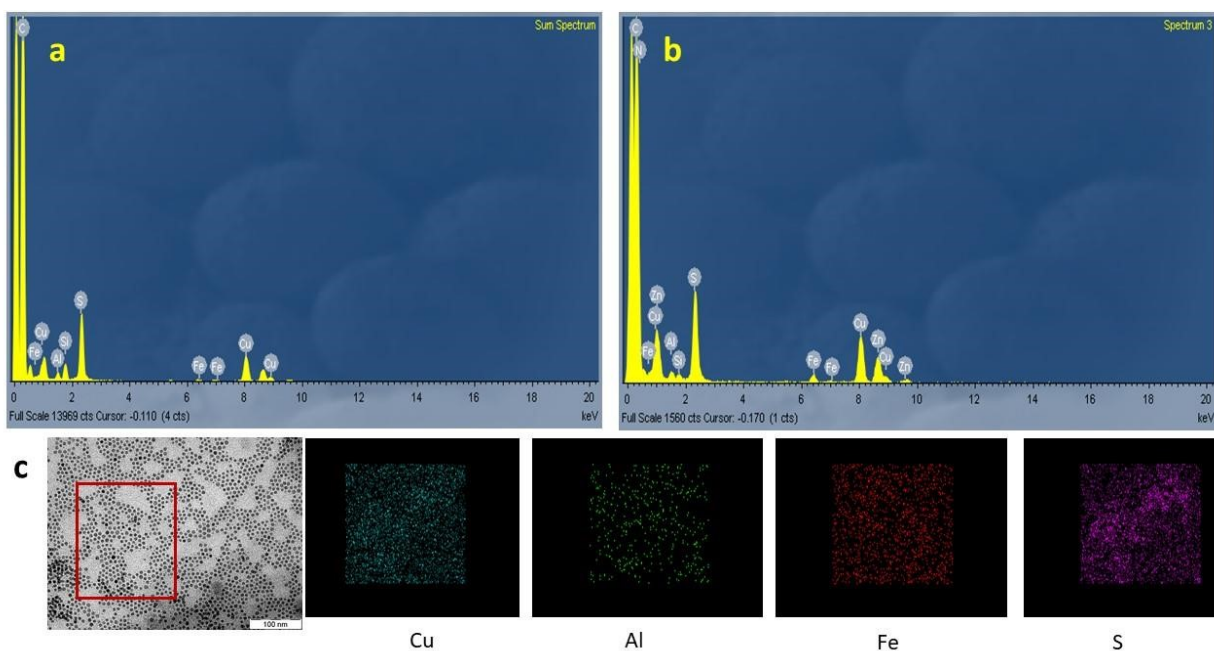


Figure 5 EDAX spectrum of alloyed $\text{CuAl}_{0.4}\text{Fe}_{0.6}\text{S}_2$ QDs (a), $\text{CuAl}_{0.4}\text{Fe}_{0.6}\text{S}_2/\text{ZnS}$ QDs (b) and STEM Elemental mapping of $\text{CuAl}_{0.4}\text{Fe}_{0.6}\text{S}_2$ QDs.

2.4.3 Optical Properties

The core material samples with different compositions of Al and Fe were prepared by similar procedure as described above. By changing the composition of aluminum and iron, it is possible to prepare $\text{CuAl}_x\text{Fe}_{1-x}\text{S}_2$ quantum dots that show absorption edges spanning from 3.5eV (bulk band gap of CuAlS_2) to 0.5 eV (bulk band gap of CuFeS_2). The direct band gap was calculated using tauc plot. Figure 6a shows the absorbance spectra of $\text{CuAl}_x\text{Fe}_{1-x}\text{S}_2$ quantum dots. It was observed that with the increase in amount of Fe, band gap of alloyed quantum dots shifted towards lower energy. The band gap of alloyed QDs is decreased because of the lowering of the conduction band minimum composed of hybrid orbitals of iron, aluminum and sulfur^{11,33}. During the change in composition the size of the quantum dots is kept constant. We have also observed size-dependent tunability in absorbance at particular chemical composition with Fe/ (Fe+Al) ratio 0.35 (Figure 6b) of alloyed QDs which confirms size confinement effect.

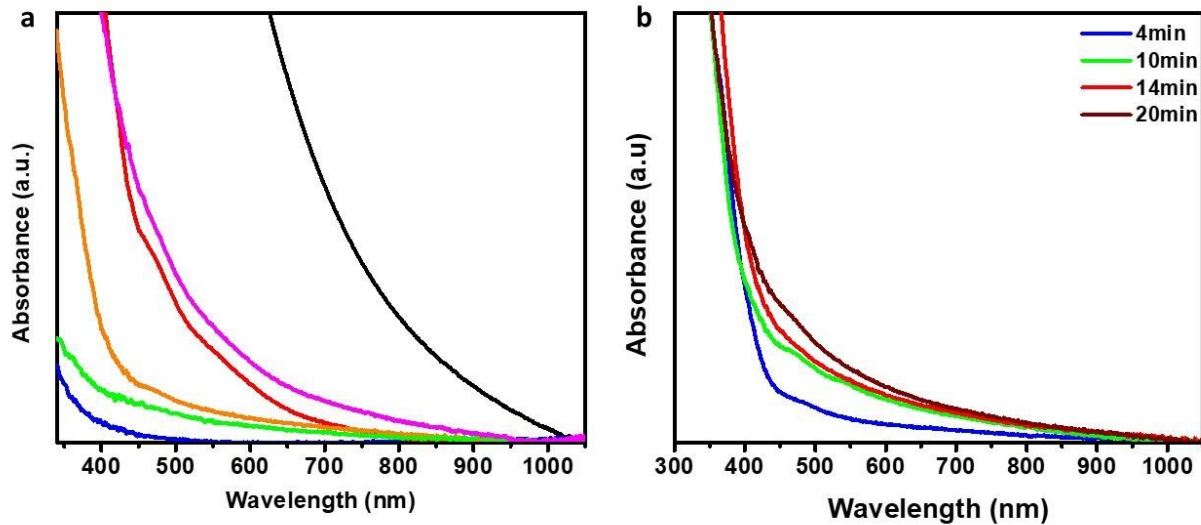


Figure 6a) absorbance spectrum of $\text{CuAl}_x\text{Fe}_{1-x}\text{S}_2$ where $1-x$ is changes as 0 (blue), 0.1(green), 0.3(orange), 0.5(red), 0.6(pink) and 1 (black). 6b) Absorbance spectrum of $\text{CuAl}_x\text{Fe}_{1-x}\text{S}_2$ with growth time at particular composition of Fe/ (Fe+Al) ratio 0.35.

Surface coating of a core semiconductor with larger energy band gap semiconductor is a well-known technique to remove surface defects. In previous studies, it is seen that elimination of the recombination sites on particle surface enhance the photoluminescence drastically. It was observed that as-prepared $\text{CuAl}_x\text{Fe}_{1-x}\text{S}_2$ alloyed quantum dots do not show any significant photoluminescence, however shell coating of ZnS lead to measureable emission ranging visible to near infrared. Higher composition of Fe (>60%) in alloy dis-stabilizes the quantum dots while surface coating, and starts leaching iron out if the reaction mixture annealed for a long time. It is observed and also reported in recent studies that $\text{CuAl}_1\text{Fe}_0\text{S}_2/\text{ZnS}$ doesn't show any luminescence due to electron transfer from core to zinc sulfide shell leading a non-radiative recombination. The incorporation of iron lowers the valance band of core and prevent the non-radiative recombination.

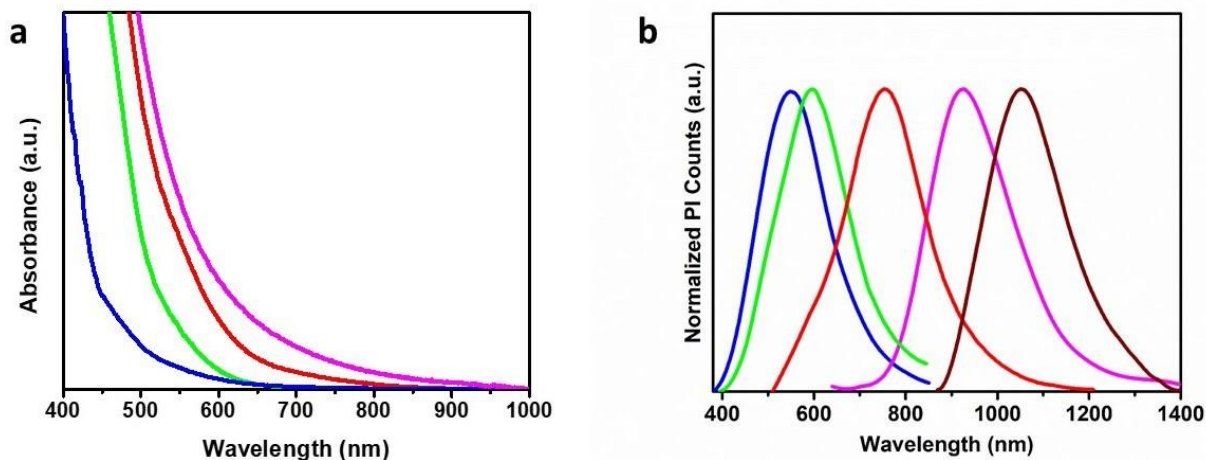


Figure: 7a Absorbance spectrum of $\text{CuAl}_x\text{Fe}_{1-x}\text{S}_2/\text{ZnS}$ with different composition of iron and aluminum. $\text{Fe}/(\text{Al}+\text{Fe})= 0.2$ (blue), 0.35 (green), 0.5 (red), 0.6 (purple) and Photoluminescence spectrum of core shell QDs respectively (figure 7b).

Figure 8a and 8b exemplifies the absorption and emission spectra of $\text{CuAl}_x\text{Fe}_{1-x}\text{S}_2/\text{ZnS}$ QDs respectively. The materials is emissive over the $554\text{-}1058$ nm ($2.23\text{-}1.17$ eV) window, with highest QYs of 3% at 600 nm emission. The Luminescence of this material in this near-IR region suggest possible application in bio-imaging.

Like other I-III-VI₂ core/shells such as $\text{CuInS}_2/\text{ZnS}$, the $\text{CuAl}_x\text{Fe}_{1-x}\text{S}_2/\text{ZnS}$ QDs also exhibit strong stokes shift relative to the band edge. In the case of CuInS_2 QDs, this stokes shift has been attributed to the occurrence of sub-gap states associated with copper. We find that the behavior of $\text{CuAl}_x\text{Fe}_{1-x}\text{S}_2/\text{ZnS}$ QDs is rather similar to that of CuInS_2 . The emission kinetics of these materials exhibit a rather unusual band gap dependence²⁸. Figure 8b shows the emission decay profile of a typical sample of $\text{CuAl}_x\text{Fe}_{1-x}\text{S}_2/\text{ZnS}$ QDs. The observed emission is broad with linewidth (200 nm, 6.2 eV) and the decay profile is homogenous and bi-exponential. Figure 8b shows the emission decay at various composition of iron and aluminium.

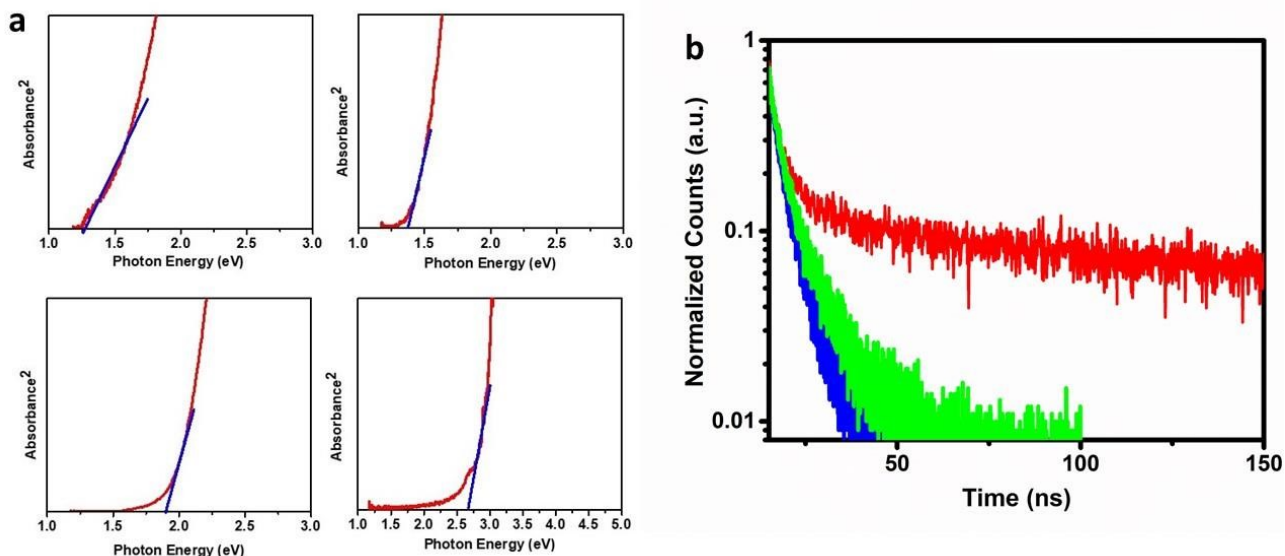


Figure: 8a Example of tauc plot which is used in calculation of direct band gap of $\text{CuAl}_x\text{Fe}_{1-x}\text{S}_2$ QDs and $\text{CuAl}_x\text{Fe}_{1-x}\text{S}_2/\text{ZnS}$ QDs. Figure 8b shows decay profile of $\text{CuAl}_x\text{Fe}_{1-x}\text{S}_2/\text{ZnS}$ QDs, Blue (554nm emission), green (603 nm emission), red (760nm emission)

These data reflect the homogeneity of the decay kinetics of this material. As the more amount of iron is incorporated, we observe that the emission lifetimes become longer suggesting involvement of defect states.

In the previous studies, a defect related emission mechanism has often been invoked for the emission behaviour of I-III-VI₂ systems⁴⁻⁶. This has been used to explain their unusually long emission lifetimes, and has been independently verified by measurements. The emissive properties of $\text{CuAl}_x\text{Fe}_{1-x}\text{S}_2/\text{ZnS}$ QDs are thus broadly similar to other I-III-VI₂ materials; the starting QDs show weak or negligible QYs, while the presence of even a thin ZnS shell causes an increase in PL emission QYs. The increase in sample lifetime could possibly arise from two different sources. The increase in wavelength of emission leads to a decrease in the available photonic density of states, partially accounting for the lengthened lifetimes. A second potential source is the involvement of a valence band defect in the $\text{CuAl}_x\text{Fe}_{1-x}\text{S}_2/\text{ZnS}$.

2.5 Conclusion

In conclusion, I have successfully synthesized the alloyed $\text{CuFe}_x\text{Al}_{1-x}\text{S}_2/\text{ZnS}$ core shell structure based quantum dots. The tetragonal chalcopyrite alloy structure was confirmed by XRD and TEM analysis. STEM elemental mapping reveals a homogenous distribution of elements. It was found that the band gap can be tune from visible to infrared making different composition and size. As prepared core material doesn't show any luminescence, however, zinc sulfide surface coating enhance the PL quantum yield which is tunable from Visible to near-IR. The maximum observed quantum yield is 3%. Incorporation of more iron leads towards longer life time suggesting the involvement of defect states. The composition of quantum dots are earth abundant and nontoxic elements making it suitable for various applications such as bio-imaging and bio-detector.

Chapter- 3

Synthesis and Characterization of CuAlS₂/Ga₂S₃

Quantum Dots

3.1 Introduction

Cadmium based quantum dots have been widely investigated due to their narrow band-edge emission^{8,24,28}. Although CdS, CdSe and other Cd alloyed II–VI semiconductor QDs have been centre of industrial research, high toxicity of cadmium is a major concern with its applications³². The replacement for the cadmium based QDs with nontoxic material which have comparable properties such as stability, small size distribution high photoluminescence quantum yield (PLQY), small linewidth emission is main focus of recent researchs^{7,15,32}. In this regard, I–III–VI₂ ternary semiconductors reveals a potential replacement for cadmium⁴⁻⁷. However, the broad PL spectra has been as a major problem⁷. The possible reasons for this broadness in PL spectrum is defects²⁴.

This chapter describes synthesis of CuAlS₂ QDs and CuAlS₂/Ga₂S₃ core/shell structures. The narrow band edge emission was achieved by coating amorphous gallium sulphide shell. While CuAlS₂ is an attractive member of the I-III-VI₂ family due to the earth abundance and benign nature of its constituent elements, its chemical and structural instability make its synthesis extremely difficult^{32,29}. Although bulk CuAlS₂ is a wide gap semiconductor³², it forms type-II heterojunctions²³ with Ga₂S₃ where the electron resides largely in the latter semiconductor. This type-II character essentially permits the tuning of the band gap of CuAlS₂/ Ga₂S₃.

3.2 Experimental Section

3.2.1 Materials

Copper chloride (CuCl, 98%), Gallium acetylacetonate {Ga₂(acac)₃, 99%}, Aluminum acetylacetonate {Al(acac)₃, 99%}, Thiourea, 1-Octadecene (ODE, technical grade 90%), Oleic acid (OA, 90%), Oleylamine (technical grade, 70%), Dodecanethiol (DDT, 98%) were purchased from Sigma-Aldrich. All the chemicals were used without any purification.

3.2.2 Synthesis

The synthesis was carried out in two steps. In first step, CuAlS₂ was prepared and in the second step, shell coating with gallium sulfide was done. All samples were prepared using slenkline technique.

In a 50 mL three necked flask, copper chloride (9.9 mg, 0.1 mM) and aluminum acetylacetonate (32.4mg, 0.1mM) were added along with 2 mL ODE as solvent and 2 mL oleic acid as ligand. The reaction mixture was heated to 100 °C under vacuum for 30 min to remove water. Further, the metal precursors were heated under argon atmosphere at 160°C for 20 min to dissolve the metal precursors. At this temperature solution turned colorless. Addition of 2 ml DDT at 180°C turned reaction mixture color to light yellow, initiating nucleation which is followed by growth. We observed that there is color change from light yellow to orange which is associated with the growth of the core material.

At deep orange color, reaction mixture was cooled down to room temperature and then shell coating was done.

The prepared QDs were cleaned by similar procedure as previous mentioned in previous chapter.

3.3 Instrumental characterization

For XRD measurement, cleaned quantum dots were dissolved in hexane (spectroscopic grade) and drop casted on a glass substrate. It formed a homogenous film. Further, the film was washed with methanol and acetone two times. A 0.154 nm Cu K α X-ray source was used to collect the data.

For TEM analysis, cleaned sample was dissolved in toluene and drop casted on copper TEM grids. HR-TEM images were obtained on a JEOL JEM-2100 transmission electron microscope (200 kV). A 250 kV TITAN TEM microscope was used for obtaining STEM.

For PI measurement, Edinburgh Instruments, FLS 920 spectrofluorimeter was used to measure emission UV-Vis region.

3.4 Result and Discussion

3.4.1 Structural Characterization

XRD pattern of prepared CuAlS₂ QDs (red thick) and gallium sulfide coated (thin red) along with standard patterns of CuAlS₂ (blue) and Ga₂S₃ (black) is shown in figure 9. As prepared CuAlS₂ QDs suggest a chalcopyrite structure, peaks corresponding to (112), (220) and (312) planes.

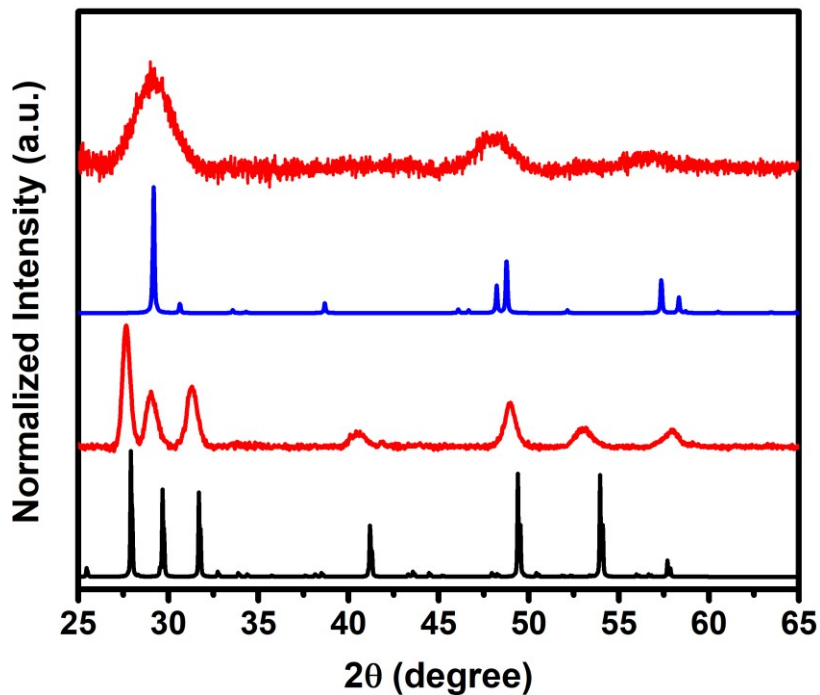


Figure 9) X-ray diffraction of CuAlS₂ (red thick), CuAlS₂/Ga₂S₃ (red thin), standard pattern of CuAlS₂ (blue) and Ga₂S₃ (black).

However, after shell coating, the observed crystal structure is wurtzite. Wurtzite is a hexagonal crystal system. Further, an elongated hexagonal structure is confirmed from TEM analysis. The XRD analysis reveals absence of any secondary copper chalcogenides.

Figure 10a and 10b show HRTEM images of CuAlS₂/ZnS QDs. The average size of CSQD CuAlS₂/Ga₂S₃ is varied 19 ± 1.6 nm. Inter-planer distance calculated from HRTEM image confirms the presence of two different crystal structures in the same QD. The (002) plane of Ga₂S₃ has an interplanar distance similar to the interplanar distance of (112) planes of CuAlS₂ (0.32 nm). The growth of Ga₂S₃ on core material CuAlS₂ can thus occur by continuity of (002) and (112) planes at the semiconductor interface. This is also shown in the FFT image (figure 9c) that reveals a well-defined alignment of planes of Ga₂S₃ and CuAlS₂ in the crystal.

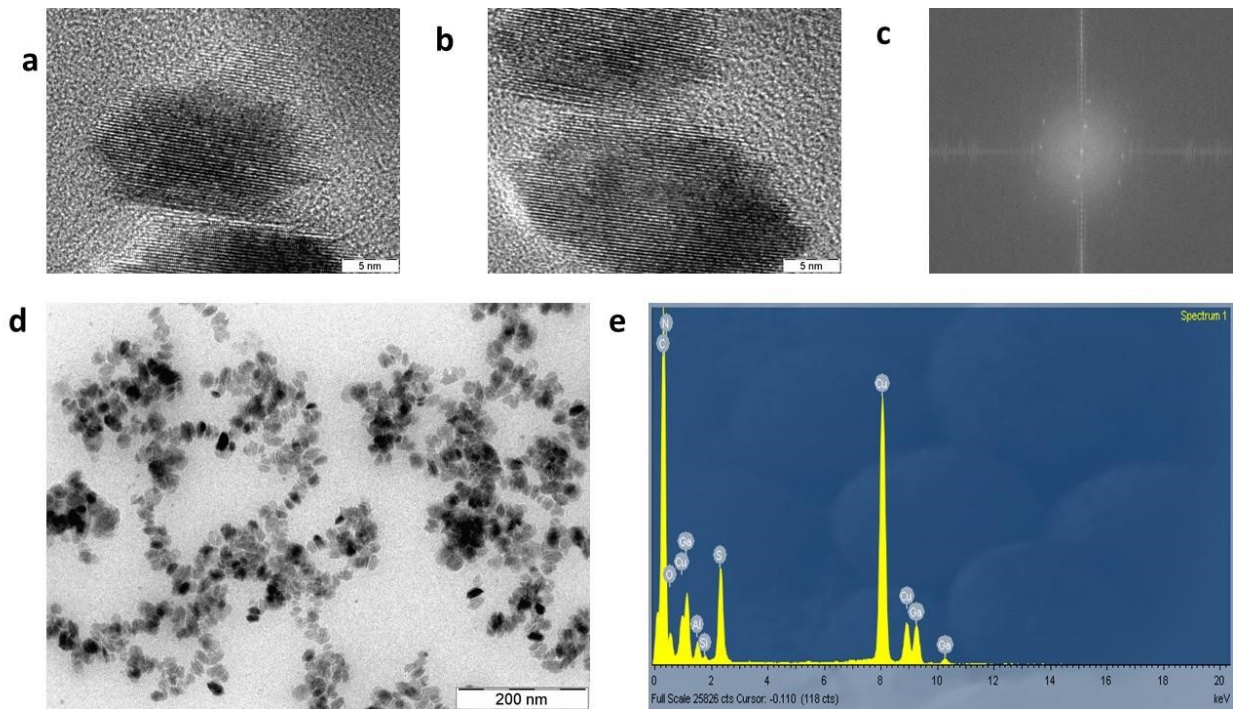


Figure 10: High resolution TEM images (a, b), TEM images, Fast Fourier Transformation (d) and EDAX spectrum of CuAlS₂/Ga₂S₃.

3.4.2 Optical Characterization

As prepared CuAlS₂ doesn't show any significant PL possibly due to surface traps sites. However coating with II-VI shell Ga₂S₃ (bulk band gap 2.8 nm) enhanced the PL. It is

reported that gallium sulfide forms an amorphous shell which improve the stability of the QDs³³. Figure 11a exemplified the absorbance spectra of CuAIS₂/Ga₂S₃ which range from 300 to 380nm over the course of 60 min of heat treatment. Figure 11b shows the PL spectrum of CuAIS₂/Ga₂S₃ spanning 360 – 390 nm. Unlikely other ternary CSQDs CuAIS₂/Ga₂S₃ reveals a narrow FWHM of 66 nm.

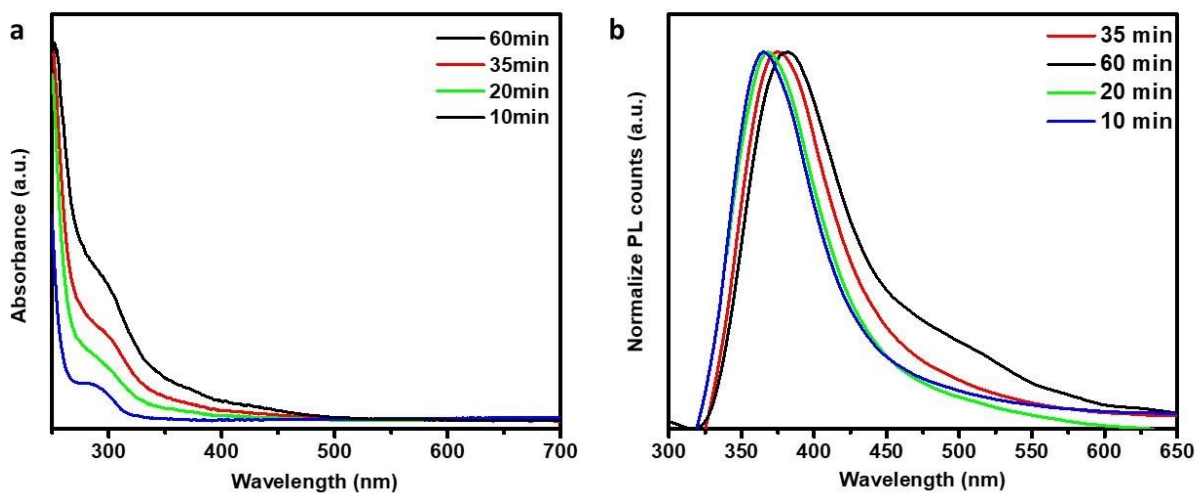


Figure 11: Absorbance spectrum (left) and photoluminescence spectrum (right) of CuAIS₂/Ga₂S₃.

3.5 Conclusion

In conclusion, we have successfully synthesized gallium sulfide coated CuAlS₂ quantum dots. The XRD data reveals that the core material has a chalcopyrite structure. As prepared core material do not show any significant photoluminescence. However, coating with Ga₂S₃ gives rise to emission from 360nm to 390nm with the change in shell thickness. More experimental investigation is needed to completely understand the structural and optical properties of the above material.

Reference

1. Kamat, P. V. Quantum Dot Solar Cells. Semiconductor Nanocrystals as Light Harvesters *J. Phys. Chem. C*, 2008, 112, 18737–18753
2. Kovalenko, M. V.; Manna, L.; Cabot, A.; Hens, Z.; Talapin, D. V.; Kagan, C. R.; Klimov, V. I.; Rogach, A. L.; Reiss, P.; Milliron, D. J.; Guyot-Sionnest, P.; Konstantatos, G.; Parak, W. J.; Hyeon, T.; Korgel, B. A.; Murray, C. B.; Heiss, W. Prospects of Nanoscience with Nanocrystals. *ACS Nano* 2015, 9, 1012–1057.
3. Keuleyan, S.; Lhuillier, E.; Brajuskovic, V.; Guyot-Sionnest, P. Mid-infrared HgTe colloidal quantum dot photodetectors *Nat. Photonics* 2011, 5, 489–493.
4. Allen, P. M.; Bawendi, M. G. Ternary I–III–VI Quantum Dots Luminescent in the Red to Near-Infrared. *J. Am. Chem. Soc.* 2008, 130, 9240–9241.
5. Li, L.; Daou, T. J.; Texier, I.; Kim Chi, T. T.; Liem, N. Q.; Reiss, P. Highly Luminescent CuInS₂/ZnS Core/Shell Nanocrystals: Cadmium-Free Quantum Dots for In Vivo Imaging. *Chem. Mater.* 2009, 21, 2422–2429.
6. Bhattacharyya, B.; Pandey, A. CuFeS₂ Quantum Dots and Highly Luminescent CuFeS₂ Based Core/Shell Structures: Synthesis, Tunability, and Photophysics. *J. Am. Chem. Soc.* 2016, 138, 10207–10213.
7. Chen, B.; Pradhan, N.; Zhong, H. From Large-Scale Synthesis to Lighting Device Applications of Ternary I–III–VI Semiconductor Nanocrystals: Inspiring Greener Material Emitters. *J. Phys. Chem. Lett.* 2018, 9, 435–445.
8. Yu, W. W.; Peng, X. Formation of High-Quality CdS and Other II–VI Semiconductor Nanocrystals in Noncoordinating Solvents: Tunable Reactivity of Monomers. *Angew. Chem., Int. Ed.* 2002, 41, 2368–2371.
9. Sharma, D. K.; Hirata, S.; Bujak, L.; Biju, V.; Kameyama, T.; Kishi, M.; Torimoto, T.; Vacha, M. Single-Particle Spectroscopy of III–VI Semiconductor Nanocrystals: Spectral Diffusion and Suppression of Blinking by Two-color Excitation. *Nanoscale* 2016, 8, 13687–13694.
10. Wegner, K.D.; Hildebrandt, N. Quantum dots: bright and versatile in vitro and in vivo fluorescence imaging biosensors. *Chem. Soc. Rev.*, 2015, 44, 4792–4834

11. Bailey, R. E.; Nie, S. Alloyed Semiconductor Quantum Dots: Tuning the Optical Properties without Changing the Particle Size. *J. Am. Chem. Soc.*, 2003, 125(23), 7100–7106.
12. Zhong, H.; Lo, S. S.; Mirkovic, T.; Li, Y.; Ding, Y.; Li, Y.; Scholes, G. D. Noninjection Gram-Scale Synthesis of Monodisperse Pyramidal CuInS₂ Nanocrystals and Their Size-Dependent Properties. *ACS Nano* 2010, 4, 5253–5262.
13. Kameyama, T.; Ishigami, Y.; Yukawa, H.; Shimada, T.; Baba, Y.; Ishikawa, T.; Kuwabata, S.; Torimoto, T. Crystal Phase-controlled Synthesis of Rod-shaped AgInTe₂ Nanocrystals for in vivo Imaging in the Near-infrared Wavelength Region. *Nanoscale* 2016, 8, 5435–5440.
14. Li, L.; Reiss, P. One-pot Synthesis of Highly Luminescent InP/ ZnS Nanocrystals without Precursor Injection. *J. Am. Chem. Soc.* 2008, 130, 11588–11589.
15. Reiss, P.; Carrière, M.; Lincheneau, C.; Vaure, L.; Tamang, S. Synthesis of Semiconductor Nanocrystals, Focusing on Nontoxic and Earth-Abundant Materials. *Chem. Rev.* 2016, 116, 10731–10819
16. Battaglia, D.; Peng, X. Formation of High Quality InP and InAs Nanocrystals in a Noncoordinating Solvent. *Nano Lett.* 2002, 2, 1027–1030.
17. Park, J.; Dvoracek, C.; Lee, K. H.; Galloway, J. F.; Bhang, H. e. C.; Pomper, M. G.; Searson, P. C. CuInSe/ZnS Core/Shell NIR Quantum Dots for Biomedical Imaging. *Small* 2011, 7, 3148–3152.
18. Panthani, M. G.; Akhavan, V.; Goodfellow, B.; Schmidtke, J. P.; Dunn, L.; Dodabalapur, A.; Barbara, P. F.; Korgel, B. A. Synthesis of CuInS₂, CuInSe₂, and Cu(In_xGa_{1-x})Se₂ (CIGS) Nanocrystal “Inks” for Printable Photovoltaics. *J. Am. Chem. Soc.* 2008, 130, 16770–16777.
19. Ghosh, S.; Avellini, T.; Petrelli, A.; Kriegel, I.; Gaspari, R.; Almeida, G.; Bertoni, G.; Cavalli, A.; Scotognella, F.; Pellegrino, T.; Manna, L. Colloidal CuFeS₂ Nanocrystals: Intermediate Fe d-Band Leads to High Photothermal Conversion Efficiency. *Chem. Mater.* 2016, 28, 4848–4858.
20. Zhang, S. B.; Wei, S.-H.; Zunger, A. A Phenomenological Model for Systematization and Prediction of Doping Limits in II–VI and I–III–VI₂ Compounds. *J. Appl. Phys.* 1998, 83, 3192–3196.

21. Regulacio, M. D.; Han, M.-Y. Multinary I-III-VI₂ and I₂-II-IVVI₄ Semiconductor Nanostructures for Photocatalytic Applications. *Acc. Chem. Res.* 2016, 49, 511–519.
22. Reiss, P.; Bleuse, J.; Pron, A. Highly Luminescent CdSe/ZnSe Core/Shell Nanocrystals of Low Size Dispersion. *Nano Lett.* 2002, 2, 781–784.
23. Zhong, H.; Scholes, G. D. Shape Tuning of Type II CdTe/CdSe Colloidal Nanocrystal Heterostructures through Seeded Growth. *J. Am. Chem. Soc.* 2009, 131, 9170–9171.
24. Xie, R.; Rutherford, M.; Peng, X. Formation of High-Quality I–III–VI Semiconductor Nanocrystals by Tuning Relative Reactivity of Cationic Precursors. *J. Am. Chem. Soc.* 2009, 131, 5691–5697.
25. Du, J.; Du, Z.; Hu, J.-S.; Pan, Z.; Shen, Q.; Sun, J.; Long, D.; Dong, H.; Sun, L.; Zhong, X.; Wan, L.-J. Zn–Cu–In–Se Quantum Dot Solar Cells with a Certified Power Conversion Efficiency of 11.6%. *J. Am. Chem. Soc.* 2016, 138, 4201–4209.
26. Song, W.-S.; Yang, H. Efficient White-Light-Emitting Diodes Fabricated from Highly Fluorescent Copper Indium Sulfide Core/ Shell Quantum Dots. *Chem. Mater.* 2012, 24, 1961–1967.
27. Leatherdale, C. A.; Woo, W. K.; Mikulec, F. V.; Bawendi, M. G. On the Absorption Cross Section of CdSe Nanocrystal Quantum Dots. *J. Phys. Chem. B* 2002, 106, 7619–7622.
28. Li, L.; Pandey, A.; Werder, D. J.; Khanal, B. P.; Pietryga, J. M.; Klimov, V. I. Efficient Synthesis of Highly Luminescent Copper Indium Sulfide-Based Core/Shell Nanocrystals with Surprisingly Long-Lived Emission. *J. Am. Chem. Soc.* 2011, 133, 1176–1179.
29. Bhattacharyya, B.; Simlandy, A. K.; Chakraborty, A.; Rajasekar, G. P.; Aetukuri, N. B.; Mukherjee, S.; Pandey, A. Efficient Photosynthesis of Organics from Aqueous Bicarbonate Ions by Quantum Dots using Visible Light. *ACS Energy Lett.* 2018, 3, 1508–1514.
30. Conejeros, S.; Alemany, P.; Lluell, M.; Moreira, I. d. P. R.; Sánchez, V. c.; Llanos, J. Electronic Structure and Magnetic Properties of CuFeS₂. *Inorg. Chem.* 2015, 54, 4840–4849.

31. Talpur, M. Y. Highly Efficient Cd-Free Alloyed Core/Shell Quantum Dots with Optimized Precursor Concentrations. *J. Phys. Chem. C*. 2016, 14, 7885-7892.
32. Bhattacharyya, B.; Pandit, T.; Rajasekar, G. P.; Pandey, A. Optical Transparency Enabled by Anomalous Stokes Shift in Visible Light-Emitting CuAlS₂ - Based Quantum Dots. *J. Phys. Chem. Lett.* 2018, 9, 4451–4456.
33. Kameyama, T.; Kishi, M.; Miyamae, C.; Sharma, D.K.; Hirata, S.; Yamamoto, T.; Uematsu, T.; Vacha, M.; Kuwabata, S.; Torimoto, T. Wavelength-Tunable Band Edge Photoluminescence of Nonstoichiometric Ag-In-S nanoparticles via Ga⁺³ Doping *ACS Appl. Mater. Interfaces* 2018, 10, 42844-42855.
34. Guillemoles, J. F.; Kronik, L.; Cahen, D.; Rau, U.; Jasenek, A.; Schock, H. W. Stability Issues of Cu(In,Ga)Se₂-based Solar Cells. *J. Phys. Chem. B* 2000, 104, 4849–4862.